ФИЗИКА ЭЛЕМЕНТАРНЫХ ЧАСТИЦ И АТОМНОГО ЯДРА
2011. Т. 42. ВЫП. 4

NEUTRINOS: DETERMINATION OF MASSES AND MIXING

M. C. Gonzalez-Garcia

Institució Catalana de Recerca i Estudis Avançats (ICREA),
Departament d'Estructura i Constituents de la Matèria and ICC-UB,
Universitat de Barcelona, Barcelona, Spain,
C. N. Yang Institute for Theoretical Physics, State University
of New York at Stony Brook, Stony Brook, NY, USA

ФИЗИКА ЭЛЕМЕНТАРНЫХ ЧАСТИЦ И АТОМНОГО ЯДРА
2011. Т. 42. ВЫП. 4

NEUTRINOS: DETERMINATION OF MASSES AND MIXING

M. C. Gonzalez-Garcia

Institució Catalana de Recerca i Estudis Avançats (ICREA),
Departament d'Estructura i Constituents de la Matèria and ICC-UB,
Universitat de Barcelona, Barcelona, Spain,
C. N. Yang Institute for Theoretical Physics, State University
of New York at Stony Brook, Stony Brook, NY, USA

The purpose of these lectures is to quantitatively summarize the present status of the determination of the masses and mixing of neutrinos. The field of neutrino phenomenology and its forward-looking perspectives are rapidly evolving, and these lectures are only a partial introduction. For more details I suggest to consult the review articles [1–12], and textbooks [13–19].

PACS: 14.60.Pq

INTRODUCTION

The Standard Model (SM) is based on the gauge symmetry $SU(3)_C \times SU(2)_L \times U(1)_Y$ spontaneously broken to $SU(3)_C \times U(1)_{\rm EM}$ by the vacuum expectations value (VEV), v, of the Higgs doublet field ϕ. The SM contains three fermion generations which reside in chiral representations of the gauge group. Right-handed fields are included for charged fermions as they are needed to build the electromagnetic and strong currents. No right-handed neutrino is included in the model since neutrinos are neutral.

In the SM, fermion masses arise from the Yukawa interactions which couple the right-handed fermion singlets to the left-handed fermion doublets and the Higgs doublet. After spontaneous electroweak symmetry breaking these interactions lead to charged fermion masses but leave the neutrinos massless. No Yukawa interaction can be written that would give a tree level mass to the neutrino because no right-handed neutrino field exists in the model.

One could think that neutrino masses could arise from loop corrections if these corrections induced effective terms $Y^\nu_{ij}/v\big(\bar{L}_{Li}\tilde{\phi}\big)\big(\tilde{\phi}^T L^C_{Lj}\big)$, where L_{Li} are the lepton doublets. This, however, cannot happen because within the SM $G^{\rm global}_{\rm SM} = U(1)_B \times U(1)_e \times U(1)_\mu \times U(1)_\tau$ is an accidental global symmetry. Here $U(1)_B$ is the baryon number symmetry, and $U(1)_{e,\mu,\tau}$ are the three-lepton

flavor symmetries. Terms of the form above violate $G_{\rm SM}^{\rm global}$ and therefore cannot be induced by loop corrections. Furthermore, they cannot be induced by nonperturbative corrections because the $U(1)_{B-L}$ subgroup of $G_{\rm SM}^{\rm global}$ is nonanomalous.

It follows then that the SM predicts that neutrinos are *strictly* massless. Consequently, there is neither mixing nor CP violation in the leptonic sector.

Therefore, if neutrinos are massive, the SM has to be extended. The lectures in [20] discussed different alternatives to extend the SM in order to introduce neutrino masses. In any of these extensions lepton flavors are mixed in the CC interactions of the leptons [27], and a leptonic mixing matrix appears equivalent to the CKM [31] matrix for the quarks. However the discussion of leptonic mixing is complicated by two factors. First, the number of massive neutrinos (n) is unknown, since there are no constraints on the number of right-handed, SM-singlet, neutrinos. Second, since neutrinos carry neither color nor electromagnetic charge, they could be Majorana fermions. As a consequence the number of new parameters in the model depends on the number of massive neutrino states and on whether they are Dirac or Majorana particles.

In general, if we denote the neutrino mass eigenstates by ν_i, $i = 1, 2, \ldots, n$, and the charged lepton mass eigenstates by $l_i = (e, \mu, \tau)$, in the mass basis, leptonic CC interactions are given by

$$-\mathcal{L}_{\rm CC} = \frac{g}{\sqrt{2}}\, \overline{l_{iL}}\, \gamma^\mu\, U_{ij}\, \nu_j\, W_\mu^+ + \text{h.c.} \tag{1}$$

Here U is a $3 \times n$ matrix $U_{ij} = P_{\ell,ii}\, {V_{ik}^\ell}^\dagger\, V_{kj}^\nu\, (P_{\nu,jj})$, where V^ℓ (3×3) and V^ν $(n \times n)$ are the diagonalizing matrix of the charged leptons and neutrino mass matrix, respectively $V^{\ell\dagger} M_\ell M_\ell^\dagger V^\ell = \text{diag}\,(m_e^2, m_\mu^2, m_\tau^2)$ and $V^{\nu\dagger} M_\nu^\dagger M_\nu V^\nu = \text{diag}\,(m_1^2, m_2^2, m_3^2, \ldots, m_n^2)$.

P_ℓ is a diagonal 3×3 phase matrix, that is conventionally used to reduce by three the number of phases in U. P_ν is a diagonal matrix with additional arbitrary phases (chosen to reduce the number of phases in U) only for Dirac states. For Majorana neutrinos, this matrix is simply a unit matrix, the reason being that if one rotates a Majorana neutrino by a phase, this phase will appear in its mass term which will no longer be real. Thus, the number of phases that can be absorbed by redefining the mass eigenstates depends on whether the neutrinos are Dirac or Majorana particles. In particular, if there are only three Majorana (Dirac) neutrinos, U is a 3×3 matrix analogous to the CKM matrix for the quarks, but due to the Majorana (Dirac) nature of the neutrinos it depends on six (four) independent parameters: three mixing angles and three (one) phases.

A consequence of the presence of the leptonic mixing is the possibility of flavour oscillations of the neutrinos. In this school we had a nice set of lectures by S. Bilenky [21] on the formalism of neutrino oscillations, where the relevant expressions for the oscillation probabilities in vacuum and in matter were derived.

In my lectures I will only discuss the status of the determination of the masses and mixing angles from the direct comparison of the expectations in the framework of neutrino oscillations with the present experimental results.

1. DOMINANT 2-ν OSCILLATIONS FOR SOLAR NEUTRINOS AND KamLAND

The simplest explanation of the solar neutrino data described in the lectures in [22] is the oscillations of ν_e into an active (ν_μ and/or ν_τ) or a sterile (ν_s) neutrino. Oscillations into pure sterile neutrinos are strongly disfavored by the SNO data because if the beam comprises of only ν_es and ν_ss, the three observed CC, ES, and NC fluxes should be equal (up to effects due to spectral distortions) — an hypothesis which is now ruled out at more than 7σ by the SNO data.

The goal of the analysis of the solar neutrino data in terms of neutrino oscillations is to determine which range of mass-squared difference and mixing angle can be responsible for the observed deficit. In order to answer this question in a statistically meaningful way one must compare the predictions in the different oscillation regimes with the observations, including all the sources of uncertainties and their correlations. In the present analysis, the main sources of uncertainty are the theoretical errors in the prediction of the solar neutrino fluxes for the different reactions as obtained within the Standard Solar Model (SSM). These errors are due to uncertainties in the twelve basic ingredients of the solar model, which include the nuclear reaction rates (parametrized in terms of the astrophysical factors S_{11}, S_{33}, S_{34}, $S_{1,14}$, and S_{17}): the solar luminosity, the metallicity Z/X, the Sun age, the opacity, the diffusion, and the electronic capture of ^{7}Be.

Indeed a new puzzle emerged in the consistency of SSMs. Till recently SSMs have had notable successes in predicting other observations. In particular, quantities measured by helioseismology such as the radial distributions of sound speeds and densities showed good agreement with the predictions of the SSM calculations and provided accurate information on the solar interior. A key element to this agreement were the input values of abundances of heavy elements on the surface of the Sun. However, recent detailed determination of the abundances of the heavy elements on the solar surface lead to lower values. A SSM which incorporates such lower metallicities fails at explaining the helioseismological observations [32]. Changes in the Sun modeling, in particular of the less known convective zone, are not able to account for this discrepancy.

So far, there has not been a successful solution of this puzzle. Thus the situation is that at present, there is no fully consistent SSM. This leads to the construction of two different sets of SSMs, one (labeled «GS») based on the older solar abundances leading to high metallicity, and one (labeled «AGSS») assuming lower metallicity as inferred from more recent determination of the

solar abundances [33]. Solar neutrino data has the potential to discriminate between these two models but not within the present precision [34].

Another source of theoretical error arises from the uncertainties in the neutrino interaction cross section for the different detection processes. Among those, recently, the SAGE collaboration has presented the results of a new calibration of the SAGE detector with a reactor-produced ^{37}Ar neutrino source. The ratio of observed to expected event rate in this experiment, once combined with the measured rates in the three prior ^{51}Cr neutrino-source experiments with Gallium, is 0.87 ± 0.05. As a possible explanation for this low result, SAGE proposed that the cross section for neutrino capture by the two lowest-lying excited states in ^{71}Ge may have been overestimated in the latest calculations of Bahcall [35]. As an alternative, the authors consider a modified capture cross section where the contribution from these two excited states is set to zero [36].

We show first in Fig. 1 the results of the analysis of the total event rates as it was in the summer of 2001 including the total rates from Chlorine, Gallium, SuperKamiokande (SK) and the first determination of the CC event rates at SNO. In the figure we plot the allowed regions which correspond to 90, 95, 99, and 99.73% (3σ) CL for ν_e oscillations into active neutrinos (2 d.o.f.). As is seen in the figure, there were several oscillation regimes compatible within errors with the

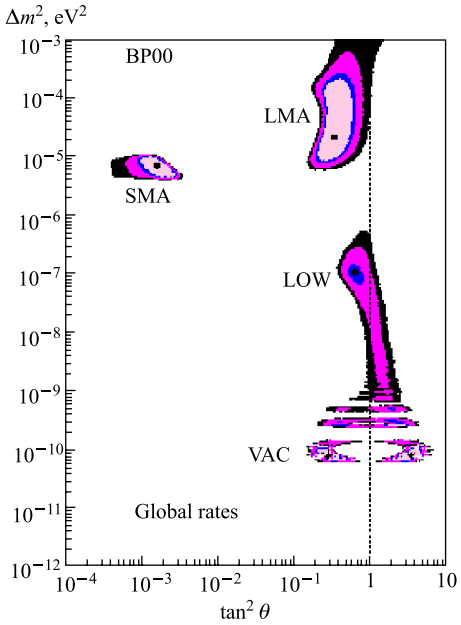

Fig. 1. Allowed oscillation parameters (at 90, 95, 99, and 99.73% CL) from the analysis of the total event rates of the Chlorine, Gallium, SK and the first SNO CC experiments

experimental data. These allowed parameter regions to be denoted as *MSW small mixing angle* (SMA), *MSW large mixing angle* (LMA), *MSW low mass* (LOW) and *vacuum oscillations* (VAC).

For the LMA solution, oscillations for the ^{8}B neutrinos occur in the adiabatic regime and the survival probability is higher for lower energy neutrinos. This situation fits well the higher rate observed at gallium experiments. For the LOW solution, the situation is opposite but matter effects in the Earth for pp and ^{7}Be neutrinos enhance the average annual survival probability for these lower energy neutrinos. The combination of these effects still allows a reasonable description of the Gallium rate. For the SMA solution the oscillations for the ^{8}B neutrinos occur in the nonadiabatic regime while for the VAC solution the oscillation wavelength is of the order of the Sun–Earth distance for ^{8}B neutrinos.

Further information on the different oscillation regimes can be obtained from the analysis of the energy- and time-dependent data from SK and SNO. For example, for LMA and LOW, the expected energy spectrum at these experiments is very little distorted. Also in the lower part of the LMA region and in the upper part of the LOW region matter effects in the Earth are important and some day–night variation is expected. For SMA, a positive slope of the energy spectrum is predicted, with larger slope for larger mixing angle within SMA. For VAC, large distortions of the energy spectrum are expected as imprints of the L/E dependence of the survival probability. The quantification of these effects depends on the precise values of the oscillation parameters.

The observed day–night spectra in SK and SNO are essentially undistorted in comparison to the SSM expectation and show no significant differences between the day and the night periods. Consequently, a large region of the oscillation parameter space where these variations are expected to be large can be excluded. In particular:

• SMA: within this region, the part with larger mixing angle fails to comply with the observed energy spectrum, while the part with smaller mixing angles gives a not good enough fit to the total rates.

• VAC: the observed undistorted energy spectrum cannot be accommodated.

• LMA and LOW: the small Δm^2 part of LMA and the LOW solution are eliminated because they predict a day–night variation that is larger than observed.

Thus with the inclusion of the time and energy dependence of the ^{8}B neutrino fluxes at SK and SNO it was possible to select the LMA as the most favored solution to the solar neutrino problem. We show in Fig. 2 the allowed region of parameters which correspond to 90, 95, 99, and 99.73% (3σ) CL for ν_e oscillations from the global analysis of the latest solar neutrino data.

These small values of Δm^2 can also be accessed in the terrestrial experiment KamLAND using as beam the $\bar{\nu}_e$s from nuclear reactors located over distances of the order of hundred kilometers. Indeed the KamLAND results can be interpreted in terms of $\bar{\nu}_e$ oscillations with parameters shown in Fig. 3.

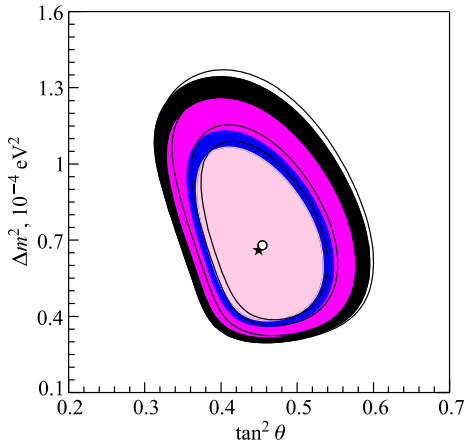

Fig. 2. Allowed oscillation parameters (at 90, 95, 99, and 99.73% CL) from the global analysis of the solar neutrino data. The full (void) regions correspond to the GS98 (AGSS09) solar models (see [37] for details)

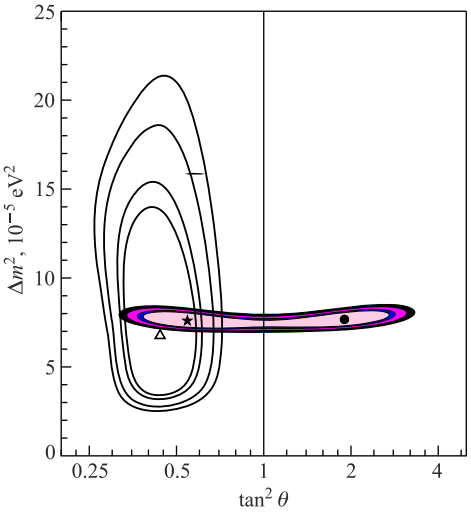

Fig. 3. Allowed oscillation parameters (at 90, 95, 99, and 99.73% CL) from the analysis of KamLAND data as compared to the allowed region of solar neutrino experiments as of 2008

The most important aspect of Fig. 3 is the demonstration by KamLAND that antineutrinos oscillate with parameters that are consistent with the LMA solution of the solar neutrino problem.

2. DOMINANT 2-ν OSCILLATIONS FOR ATMOSPHERIC AND LBL NEUTRINOS

The atmospheric neutrino data is described in detail in the lectures in [23] while for Long Baseline (LBL) experiments, K2K and MINOS I refer to the lectures in [24].

The simplest and most direct interpretation of the atmospheric neutrino data is that of muon neutrino oscillations. The required value of the oscillation parameters can be easily estimated from the following observations:

• The angular distribution of contained events shows that, for $E \sim 1$ GeV, the deficit comes mainly from $L \sim 10^2$–10^4 km. The corresponding oscillation phase must be maximal, $\dfrac{\Delta m^2(\mathrm{eV}^2)L(\mathrm{km})}{2E(\mathrm{GeV})} \sim 1$, which requires $\Delta m^2 \sim 10^{-4}$–10^{-2} eV^2.

• Assuming that all upgoing ν_μs, which would lead to multi-GeV events, oscillate into a different flavor while none of the downgoing ones do, the up-down asymmetry is given by $|A_\mu| = \sin^2 2\theta/(4 - \sin^2 2\theta)$. The present one sigma bound reads $|A_\mu| > 0.27$ which requires that the mixing angle is close to maximal, $\sin^2 2\theta > 0.85$.

In order to go beyond these rough estimates, one must compare in a statistically meaningful way the experimental data with the theoretical expectations. In order to do so one must account for all sources of uncertainties. They include the theoretical errors in the angular and energy dependence of the atmospheric fluxes, the uncertainties on the different type of reaction cross sections in the detection, together with the long list of experimental systematic uncertainties. The most up-to-date details on our determination of the expected rates in SK and the corresponding statistical analysis can be found in Appendix of [12].

Altogether the best interpretation of the atmospheric neutrino data is the oscillation of ν_μ into ν_τ. In Fig. 4 we plot the allowed regions from the global analysis of atmospheric data in this framework.

Other oscillation channels are presently ruled out. $\nu_\mu \to \nu_e$ is excluded with high CL as the explanation to the atmospheric neutrino anomaly for two different reasons: (i) SK high precision data show that the ν_e contained events are very well described by the SM prediction both in normalization and in their zenith angular dependence; (ii) Explaining the atmospheric data with $\nu_\mu \to \nu_e$ transition has direct implications for the $\bar{\nu}_e \to \bar{\nu}_\mu$ transition. In particular, there should be a $\bar{\nu}_e$ deficit in the CHOOZ reactor experiment which was not observed [38].

$\nu_\mu \to \nu_s$ is also ruled out as a possible explanation of the atmospheric neutrino anomaly because the presence of matter effects in this channel predicts a flatter-than-observed angular distribution of through-up-going muon events. Also if ν_μ oscillates into sterile neutrinos, one expects a relative suppression of the NC signal which has not been observed. Furthermore, SuperKamiokande has

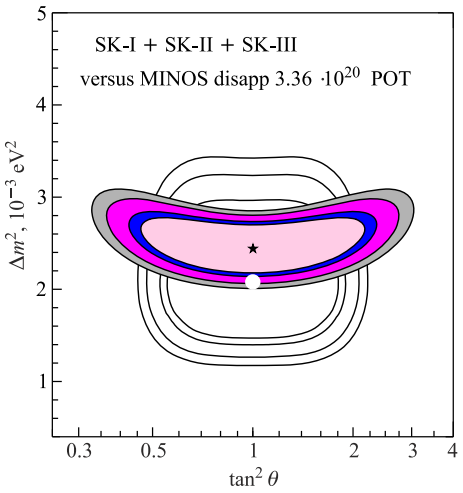

Fig. 4. Allowed regions from the analysis of MINOS (full regions) and from ATM neutrinos at the same CL (lines) (see [37] for details)

performed a dedicated analysis for the search for the effects of appearance of tau neutrinos, which disfavors the hypothesis of no ν_τ appearance.

The results of the LBL experiments K2K and MINOS confirm, both in the observed deficit of events and in their energy dependence, that accelerator ν_μ oscillate over distances of several hundred kilometers as expected from oscillations with the parameters previously inferred from the atmospheric neutrino data. This is quantitatively illustrated in Fig. 4 where we show the results of our analysis of the ATM and MINOS data, respectively. As is seen in the figure, MINOS provides an independent determination of the relevant Δm^2 while the mixing angle is still better determined by the atmospheric neutrino data.

3. SUBDOMINANT 3-ν OSCILLATION EFFECTS

From the results previously described it is obvious that the minimum joint description of solar and atmospheric evidences requires that all three known neutrinos take part in the oscillations. In this case, the mixing parameters are encoded in the 3×3 lepton mixing matrix [27, 31] which can be conveniently parametrized in the standard form

$$U = \begin{pmatrix} c_{12}\, c_{13} & s_{12}\, c_{13} & s_{13}\, \mathrm{e}^{-i\delta_{CP}} \\ -s_{12}\, c_{23} - c_{12}\, s_{13}\, s_{23}\, \mathrm{e}^{i\delta_{CP}} & c_{12}\, c_{23} - s_{12}\, s_{13}\, s_{23}\, \mathrm{e}^{i\delta_{CP}} & c_{13}\, s_{23} \\ s_{12}\, s_{23} - c_{12}\, s_{13}\, c_{23}\, \mathrm{e}^{i\delta_{CP}} & -c_{12}\, s_{23} - s_{12}\, s_{13}\, c_{23}\, \mathrm{e}^{i\delta_{CP}} & c_{13}\, c_{23} \end{pmatrix}. \quad (2)$$

The determination of the oscillation probabilities for both solar and atmospheric neutrinos requires that one solves the evolution equation of the neutrino system in the matter background of the Sun and the Earth. In the three-flavor framework, the equation in the flavor basis can be written as

$$i\frac{d\boldsymbol{\nu}}{dx} = H\,\boldsymbol{\nu}, \qquad H = U \cdot H_0^d \cdot U^\dagger + V, \tag{3}$$

where U is the lepton mixing matrix, $\boldsymbol{\nu} \equiv (\nu_e,\, \nu_\mu,\, \nu_\tau)^T$ and

$$H_0^d = H_m - \frac{m_1}{2E} = \frac{1}{2E}\mathrm{diag}\left(0,\, \Delta \mathrm{m}^2_{21},\, \Delta \mathrm{m}^2_{31}\right). \tag{4}$$

V is the effective potential that describes CC forward interactions in matter.

In total, the three-neutrino oscillation analysis involves six parameters: two mass differences (including two possible signs for one of them), three mixing angles and one CP phase.

Without loss of generality one can choose the mass differences as shown in Fig. 5 so that Δm^2_{21} is always positive and there are two possible mass orderings which we denote as *normal* and *inverted* and which correspond to the two possible choices of the sign of Δm^2_{31}. In this convention, the angles θ_{ij} can be taken without loss of generality to lie in the first quadrant, $\theta_{ij} \in [0, \pi/2]$ and the phases $\delta_{CP},\, \eta_i \in [0, 2\pi]$.

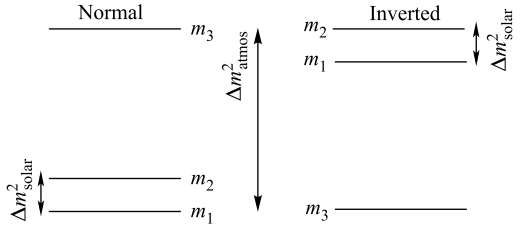

Fig. 5. Mass schemes for 3ν oscillations

The normal ordering is naturally related to hierarchical masses, $m_1 \ll m_2 \ll m_3$, for which $m_2 \simeq \sqrt{\Delta m^2_{21}}$ and $m_3 \simeq \sqrt{\Delta m^2_{32}}$, or to quasi-degenerate masses, $m_1 \simeq m_2 \simeq m_3 \gg \Delta m^2_{21}, \Delta m^2_{32}$. On the other hand, the inverted ordering implies that $m_3 < m_1 \simeq m_2$.

With this assignment Δm^2_{21} and the mixing angle θ_{12} have been chosen to be those that give the dominant oscillations for solar neutrinos while Δm^2_{31}, Δm^2_{32}, and θ_{23} give the dominant oscillation for atmospheric neutrinos.

Generic three-neutrino oscillation effects are:

- mixing effects because of the additional angle θ_{13};
- difference between normal and inverted schemes;

- coupled oscillations with two different oscillation lengths;
- CP violating effects.

The strength of these effects is controlled by the values of the ratio of mass differences, the mixing angle θ_{13}, and the CP phase δ_{CP}.

In this respect, as we have seen in the previous sections, the parameter space of solutions for solar and atmospheric oscillations in Figs. 3 and 4 satisfies

$$\Delta m^2_{21} = \Delta m^2_{\odot} \ll \Delta m^2_{\text{atm}} = |\Delta m^2_{31}| \simeq |\Delta m^2_{32}|. \tag{5}$$

This hierarchy implies that even though, in general, the transition probabilities present an oscillatory behavior with two oscillation lengths, in present experiments, such interference effects are not very visible.

The most severe limitation on the value of θ_{13} arises from the nonobservation of $\bar{\nu}_e$ disappearance at the CHOOZ reactor experiment [38]. In our notation, the survival probability of reactor antineutrinos at CHOOZ takes the form:

$$P^{\text{CHOOZ}}_{ee} \simeq 1 - \sin^2 2\theta_{13} \sin^2 \left(\frac{\Delta m^2_{31} L}{4E} \right), \tag{6}$$

where we have used that for the relevant values of energy and distance, one can safely neglect Earth matter effects and the *simeq* holds under the approximation $\Delta m^2_{21} \ll E/L$ which can be safely made for $\Delta m^2_{21} \leqslant 3 \cdot 10^{-4}$ eV^2. Thus effectively the analysis of the CHOOZ reactor data involves two oscillation parameters, the mass difference which drives the dominant atmospheric and MINOS oscillations, Δm^2_{31}, and the angle θ_{13} which is severely constrained.

3.1. Effects of θ_{13} in Solar Neutrinos and KamLAND. We first notice that $L^{\text{osc}}_{31} = 4\pi E/\Delta m^2_{31}$ is much shorter than the distance between the Sun and the Earth for solar neutrinos or between the reactors and the detectors in KamLAND. Consequently, the oscillations related to $L^{\text{osc}}_{0,31}$ are averaged. The relevant survival probability is

$$P^{3\nu}_{ee} = \sin^4 \theta_{13} + \cos^4 \theta_{13} P^{2\nu}_{ee}(\Delta m^2_{21}, \theta_{12}). \tag{7}$$

For solar neutrinos, one must also take into account the three-neutrino mixing effects in the evolution in matter. In this case, a second simplification occurs since, for the evolution in both the Sun and the Earth, $\Delta m^2_{31} \gg 2\sqrt{2} G_F n_e E \sin^2 2\theta_{13}$. Consequently, matter effects on the evolution of ν_3 can be neglected. The net result is that for solar neutrinos the survival probability can also be written as Eq. (7) with $P^{2\nu}_{ee}$ obtained taking into account evolution in the effective density:

$$n_e \Rightarrow n_e \cos^2 \theta_{13}. \tag{8}$$

For $10^{-5} \lesssim \Delta m^2/\mathrm{eV}^2 \lesssim 10^{-4}$, $P_{ee}^{2\nu}(\Delta m^2_{21}, \theta_{12})$ presents the following asymptotic behaviors:

$$P_{ee}^{2\nu}(\Delta m^2_{21}, \theta_{12}) \simeq 1 - \frac{1}{2}\sin^2(2\theta_{12}) \qquad \text{for} \quad E_\nu \lesssim \text{few} \times 100 \text{ keV}, \tag{9}$$

$$P_{ee}^{2\nu}(\Delta m^2_{21}, \theta_{12}) \simeq \sin^2(\theta_{12}) \qquad \text{for} \quad E_\nu \gtrsim \text{few} \times 1 \text{ MeV}. \tag{10}$$

The impact of the inclusion of a nonzero value of θ_{13} in the solar analysis is shown in Fig. 6 where we show the allowed regions (at 95% CL) in the $(\Delta m^2_{21}, \tan^2\theta_{12})$ plane as obtained from the analysis of low-energy (radiochemical and Borexino-LE) and high-energy (SK, SNO and Borexino-HE) solar experiments, for different values of θ_{13}. As described in Eq. (7), for fixed values of Δm^2_{21} and θ_{12}, the inclusion of a small value of θ_{13} results into a decrease on the predicted rates at a given solar neutrino experiment. This decrease can be compensated by a shift of Δm^2_{21} and θ_{12} which lead to an increase of $P_{ee}^{2\nu}$. However, the sign of the shift strongly depends on the characteristic energy of the detected neutrinos. For experiments detecting neutrinos with energies low enough for matter effects to be irrelevant (such as Chlorine and Gallium experiments), $P_{ee}^{2\nu}$ is given by Eq. (9) and increases as θ_{12} decreases. Conversely, for experiments detecting neutrinos mostly in the regime of adiabatic matter oscillations (such as SK and SNO), $P_{ee}^{2\nu}$ is given by Eq. (10) and increases as θ_{12} increases. Consequently the global solar neutrino fit worsens with θ_{13}.

3.2. Combination with KamLAND: The Hint of $\theta_{13} \neq 0$. We show in Fig. 7, *a*, *c* the present determination of the leading parameters Δm^2_{21} and θ_{12} (for $\theta_{13} = 0$) from the analysis of KamLAND spectral data compared to those from the updated solar analysis for the two solar models considered. While the results show perfect agreement in Δm^2_{21}, there appears to be a mismatch in the favored value of θ_{12} as determined from KamLAND compared to the one from solar neutrinos, this last one being mostly sensitive to the precise value of CC/NC event (i.e., to $\langle P_{ee}\rangle \propto \sin^2\theta_{12}$) as determined by SK and SNO.

This mismatch can be lifted by a nonzero value of θ_{13} [39]. This happens because, as discussed above, the CC/NC event rate can be fitted with a higher value of θ_{12} provided that a nonzero θ_{13} is included. Conversely for KamLAND Eq. (7) also holds with

$$P_{ee}^{2\nu,\mathrm{kam}} = 1 - \frac{1}{2}\sin^2(2\theta_{12})\sin^2\frac{\Delta m^2_{21} L}{2E}. \tag{11}$$

So for $\theta_{13} > 0$ the KamLAND spectrum can be well fitted with a smaller value of θ_{12}, and consequently the best-fit values for solar and KamLAND analysis agree better for $\theta_{13} \neq 0$. This behavior is clearly visible in Fig. 7, *b*, *d*. The best-fit value of θ_{12} for solar neutrino fit within the AGSS09 model is slightly larger than for the GS98 model, and therefore the required value of θ_{13} to achieve agreement with KamLAND is smaller for the AGSS09 model.

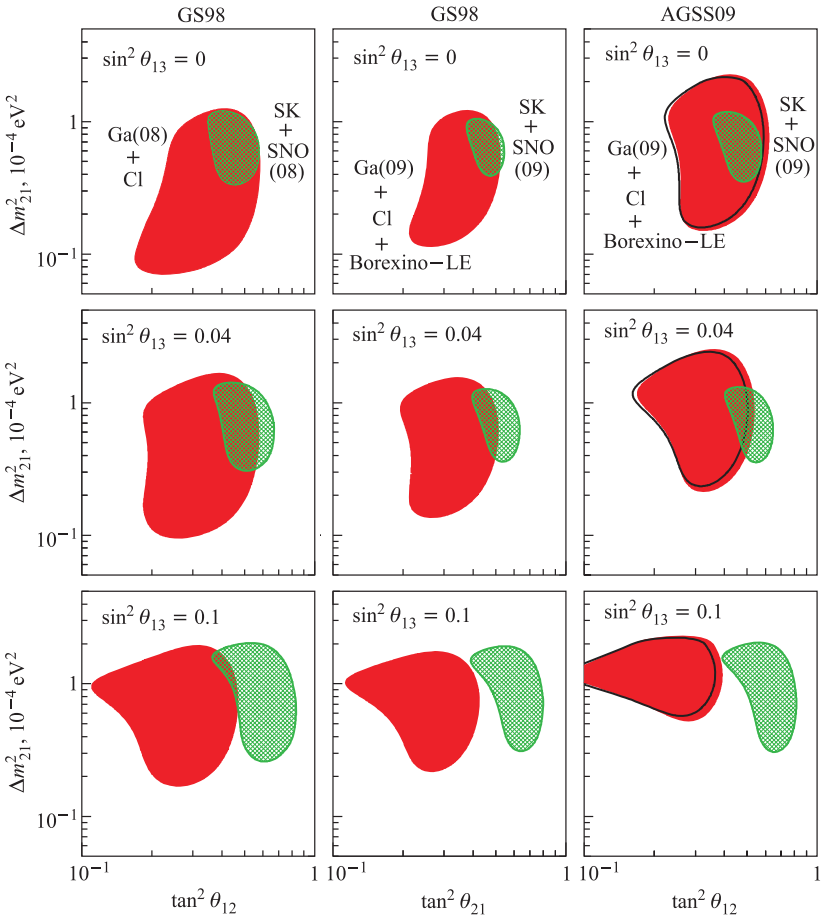

Fig. 6. Dependence on θ_{13} of the allowed (Δm^2_{21}, $\tan^2\theta_{12}$) regions (at 95% CL for 2 d.o.f.) from the partial analysis of the «low energy» and «high energy»solar neutrino data. The left column corresponds to the analysis prior to the inclusion of the latest Ga capture rate of SAGE, the energy spectrum of Borexino, and the low energy threshold analysis of the combined SNO phase I and phase II. In the central and right columns the results of those experiments are included. The central column corresponds to GS98 solar model fluxes and Gallium capture cross section of Bahcall. In the right panels, the AGSS09 solar model fluxes are used. The full (void) regions are obtained with Gallium capture cross section of Bahcall (and modified cross section advocated by the SAGE collaboration) (see [37] for details)

However, one must notice that the better agreement between the solar and KamLAND analysis for $\theta_{13} \neq 0$ has to be contrasted with the worsening of the global description of the solar neutrino data previously described.

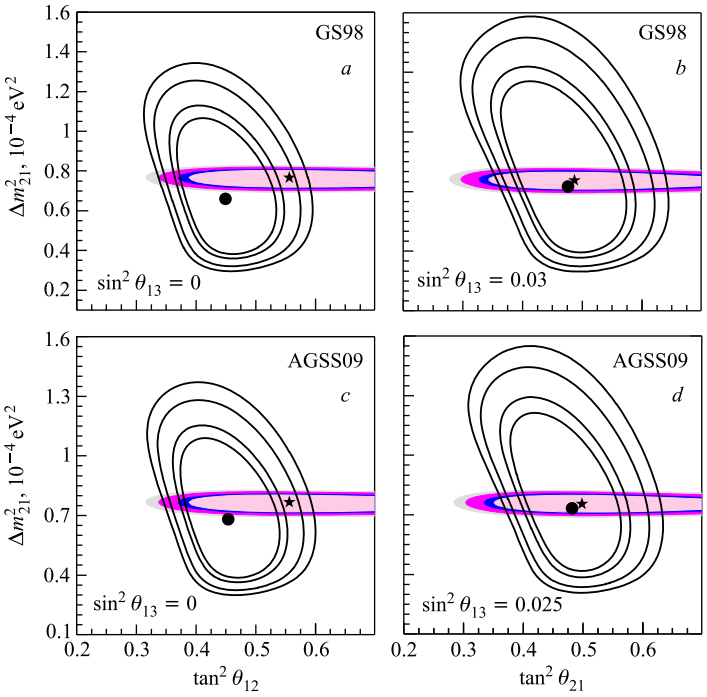

Fig. 7. Allowed parameter regions (at 90, 95, 99, and 99.73% CL for 2 d.o.f.) from analysis of KamLAND (full regions with best-fit marked by a star) and solar (void regions with best-fit marked by a dot) data for two values of θ_{13} as labeled in the figure and for the two solar models (see [37] for details)

3.3. Effects of θ_{13} in Atmospheric and LBL Neutrinos. We discuss first the subleading effect due to the mixing angle θ_{13} which is particularly easy to treat in the *hierarchical approximation* in which Δm^2_{21}-induced oscillations are neglected in the atmospheric neutrino analysis (see [12] for a list of the original references where these effects were first discussed). In this approximation one can rotate away the angle θ_{12}. Thus the resulting survival probabilities do not depend on Δm^2_{21} and θ_{12}. For instance, for constant Earth matter density with potential V_e, the various $P_{\alpha\beta}$ can be written as follows:

$$P_{ee} = 1 - 4s^2_{13,m}c^2_{13,m}\,S_{31}, \tag{12}$$

$$P_{\mu\mu} = 1 - 4s^2_{13,m}c^2_{13,m}s^4_{23}\,S_{31} - 4s^2_{13,m}s^2_{23}c^2_{23}\,S_{21} - 4c^2_{13,m}s^2_{23}c^2_{23}\,S_{32}, \tag{13}$$

$$P_{e\mu} = 4s^2_{13,m}c^2_{13,m}s^2_{23}\,S_{31}. \tag{14}$$

Here θ_{13}^m is the effective mixing angle in matter:

$$\sin 2\theta_{13}^m = \frac{\sin 2\theta_{13}}{\sqrt{(\cos 2\theta_{13} - 2EV_e/\Delta m_{31}^2)^2 + (\sin 2\theta_{13})^2}} \tag{15}$$

and S_{ij} are the oscillating factors in matter:

$$S_{ij} = \sin^2\left(\frac{\Delta\mu_{ij}^2}{4E}L\right). \tag{16}$$

In Eq. (16), $\Delta\mu_{ij}^2$ are the effective mass-squared differences in matter:

$$\Delta\mu_{21}^2 = \frac{\Delta m_{31}^2}{2}\left(\frac{\sin 2\theta_{13}}{\sin 2\theta_{13}^m} - 1\right) - EV_e, \tag{17}$$

$$\Delta\mu_{32}^2 = \frac{\Delta m_{31}^2}{2}\left(\frac{\sin 2\theta_{13}}{\sin 2\theta_{13}^m} + 1\right) + EV_e, \tag{18}$$

$$\Delta\mu_{31}^2 = \Delta m_{31}^2 \frac{\sin 2\theta_{13}}{\sin 2\theta_{13}^m}, \tag{19}$$

and L is the path length of the neutrino within the Earth.

The main effect of θ_{13} is that now atmospheric neutrinos can oscillate simultaneously in both the $\nu_\mu \to \nu_\tau$ and $\nu_\mu \to \nu_e$ (and, similarly, $\nu_e \to \nu_\tau$ and $\nu_e \to \nu_\mu$) channels. The oscillation amplitudes for channels involving ν_e are controlled by the size of $\sin^2\theta_{13} = |U_{e3}|^2$. Furthermore, because of matter effects the size of the effect is different for normal and inverted hierarchies.

In Fig. 8, we show the expected zenith angular distribution of contained e-like events (normalized to the no-oscillation expectation) for $\sin^2\theta_{13} = 0.04$. The figure shows the effect is most relevant for multi-GeV neutrinos and larger for the normal-hierarchy than inverted orderings. Also the effect can be a decrease or increase of the expected number of events with respect to the $\theta_{13} = 0$ prediction depending on whether θ_{23} is in the first or second octant. From Eqs. (12)–(14) it is easy to show that for the case of constant matter density the expected flux of ν_e events in the hierarchical approximation can be written as

$$\frac{N_e}{N_{e0}} - 1 = \langle P_{e\mu}\rangle\, \bar{r}\left(s_{23}^2 - \frac{1}{\bar{r}}\right), \tag{20}$$

where $\langle P_{e\mu}\rangle$ is the corresponding probability, Eq. (14), averaged over energy and zenith angle, and $\bar{r} = \Phi_{\mu 0}/\Phi_{e0}$ is the ratio of the electron and muon neutrino fluxes in the absence of oscillations in the relevant energy and angular bin.

For instance, for sub-GeV events $\bar{r} \sim 2$. So the effect cancels for maximal θ_{23}. For θ_{23} in the first octant ($s_{23}^2 < 0.5$) there is a decrease in the number of

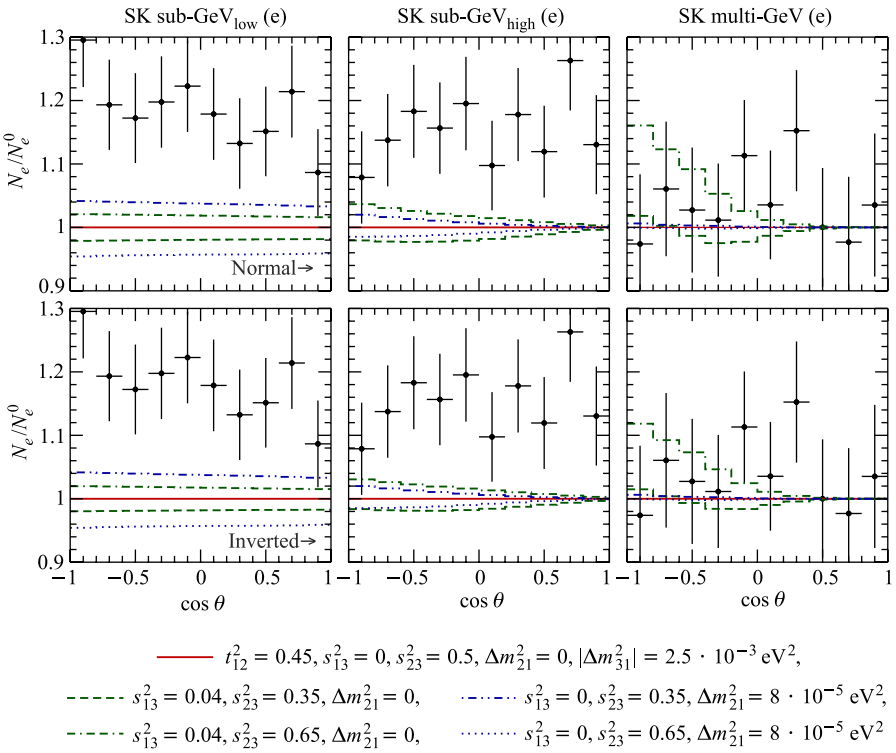

Fig. 8. Comparison of the subleading effects due to Δm^2_{21}- and θ_{13}-induced ν_e oscillations in the expected zenith angular distribution of e-like events

electron events as compared to the θ_{13} case while the opposite holds for θ_{23} in the second octant. Thus the effect is suppressed for maximal θ_{23} mixing.

For multi-GeV events, matter effects lead to an enhancement of the effect which is slightly larger for the normal ordering where the matter enhancement is in the neutrino channel. For sub-GeV events, the matter term can be neglected and the effect of a nonvanishing θ_{13} is smaller and it is the same for normal and inverted ordering.

For K2K and MINOS, matter effects can be neglected and the relevant survival probability takes the form

$$P_{\mu\mu}^{\mathrm{K2K,MINOS}} = 1 - 4\left(s_{23}^4 s_{13}^2 c_{13}^2 + c_{13}^2 s_{23}^2 c_{23}^2\right)\sin^2\left(\frac{\Delta m_{31}^2}{4E}L\right) \simeq$$

$$\simeq s_{13}^2 \frac{\cos 2\theta_{23}}{c_{23}^2} + \left(1 - s_{13}^2 \frac{\cos 2\theta_{23}}{c_{23}^2}\right) P_{\mu\mu}^{\mathrm{K2K},2\nu}(\Delta m_{31}^2, \theta_{23}) + \mathcal{O}(s_{13}^4). \quad (21)$$

So we find that in the approximation of Eq. (5), the analysis of the atmospheric and K2K + MINOS data constrains three of the six independent oscillation parameters: Δm^2_{31}, θ_{23}, and θ_{13} and for atmospheric neutrinos also the sign of Δm^2_{31} is relevant. Consequently in this approximation the mixing angle θ_{13} is the only parameter common to both solar + KamLAND and atmospheric + K2K neutrino oscillations and which may potentially allow for some mutual influence.

3.4. Effects due to Δm^2_{21} in Atmospheric Neutrinos. We next discuss the subleading effects due to Δm^2_{21} oscillations for vanishing small value of θ_{13} (see [12] for a list of the original references where these effects were first discussed). In this approximation and for constant Earth matter density the relevant oscillation probabilities can be written as

$$P_{ee} = 1 - P_{e2}, \tag{22}$$

$$P_{e\mu} = c^2_{23} P_{e2}, \tag{23}$$

$$P_{\mu\mu} = 1 - c^4_{23} P_{e2} - 2 s^2_{23} c^2_{23} \left[1 - \sqrt{1 - P_{e2} \cos\phi} \right], \tag{24}$$

where

$$P_{e2} = \sin^2 2\theta_{12,m} \sin^2 \left(\frac{\Delta m^2_{21}\, L}{4E} \frac{\sin 2\theta_{12}}{\sin 2\theta_{12,m}} \right), \tag{25}$$

with

$$\sin 2\theta_{12,m} = \frac{\sin 2\theta_{12}}{\sqrt{\left(\cos 2\theta_{12} \mp \dfrac{2EV_e}{\Delta m^2_{21}} \right)^2 + \sin^2 2\theta_{12}}}, \tag{26}$$

$$\phi \approx (\Delta m^2_{31} + s^2_{12}\, \Delta m^2_{21}) \frac{L}{2E}. \tag{27}$$

In Fig. 8 we show the angular distribution of atmospheric ν_e for nonvanishing values of Δm^2_{21} or θ_{13}. As seen in these figures, unlike for θ_{13}, the main effect of a small but nonvanishing Δm^2_{21} is mostly observable for sub-GeV electrons, and it can result either in an increase or in a decrease of the expected number of events with respect to the $\Delta m^2_{21} = 0$ prediction depending on whether θ_{23} is in the first or second octant. This behavior can be understood in terms of the approximate analytical expressions:

$$\frac{N_e}{N_{e0}} - 1 = \langle P_{e2} \rangle\, \bar{r} \left(c^2_{23} - \frac{1}{\bar{r}} \right), \tag{28}$$

$$\frac{N_\mu - N_\mu(\Delta m^2_{21} = 0)}{N_{\mu 0}} = -\langle P_{e2} \rangle\, c^2_{23} \left(c^2_{23} - \frac{1}{\bar{r}} \right), \tag{29}$$

where N_{e0} and $N_{\mu 0}$ are the expected number of electron and muon-like events in the absence of oscillations in the relevant energy and angular bin and $N_\mu(\Delta m^2_{21} = 0)$ is the expected number of muon-like events for $\Delta m^2_{21} = 0$. For sub-GeV events $\Delta m^2 \ll 2EV_e$, so

$$P_{e2} = \sin^2 2\theta_{12} \left(\frac{\Delta m^2_{21}}{2EV_e}\right)^2 \sin^2 \frac{V_e L}{2}. \tag{30}$$

According to Eqs. (28) and (29) the sign of the shift in the number of predicted events is opposite for electron and muon-like events and it depends on the factor $c^2_{23} - 1/\bar{r} \sim c^2_{23} - 0.5$. So the effect cancels for maximal θ_{23}. For θ_{23} in the first octant, $c^2_{23} > 0.5$, there is an increase (decrease) in the number of electron (muon) events as compared to the $\Delta m^2_{21} = 0$ case. For θ_{23} in the second octant the opposite holds (this is the opposite behavior than the one due to $\theta_{13} \neq 0$ previously discussed). We also see that the net shift is larger for electron events than for muon events by a factor $c^2_{23}/\bar{r}$. In summary for sub-GeV electrons, the shift in the expected number of events is proportional to the deviation of θ_{23} from maximal mixing and to $(\Delta m^2_{21})^2$, it is very weakly dependent on the zenith angle, and it decreases with the energy.

3.5. Interference of θ_{13} and Δm^2_{21} Effects. Finally we comment on the possible effects due to the interference between θ_{13}- and Δm^2_{21}-induced oscillations (see [12] for a list of the original references where these effects were first discussed) which could give sensitivity to the CP violating phase δ_{CP}. This effect is most important for sub-GeV energies for which one can write:

$$\frac{N_e}{N^0_e} - 1 \simeq \langle P_{e2}\rangle\, \bar{r} \left(c^2_{23} - \frac{1}{\bar{r}}\right) + 2\tilde{s}^2_{13}\, \bar{r} \left(s^2_{23} - \frac{1}{\bar{r}}\right) - \\ - \bar{r}\tilde{s}_{13}\tilde{c}^2_{13} \sin 2\theta_{23} \left(\cos\delta_{CP}\langle R_2\rangle - \sin\delta_{CP}\langle I_2\rangle\right), \tag{31}$$

where

$$P_{e2} = \sin^2 2\theta_{12,m}\, \sin^2 \frac{\phi_m}{2}, \tag{32}$$

$$R_2 = -\sin 2\theta_{12,m} \cos 2\theta_{12,m}\, \sin^2 \frac{\phi_m}{2}, \tag{33}$$

$$I_2 = -\frac{1}{2} \sin 2\theta_{12,m}\, \sin\phi_m, \tag{34}$$

$$\tilde{\theta}_{13} \approx \theta_{13} \left(1 + \frac{2E\, V_e}{\Delta m^2_{31}}\right). \tag{35}$$

Here ϕ_m is the phase oscillation in matter and $\theta_{12,m}$ is 12 the mixing angle in matter (Eq. (26)). As is seen from Eq. (31), the interference term (third term in

the equation) is not suppressed for maximal θ_{23} so it can dominate for θ_{23} near maximal. Also it is proportional to $\sin 2\theta_{23}$ and therefore it is not sensitive to the octant of θ_{23}.

3.6. $\nu_\mu \to \nu_e$ Appearance Results in MINOS. As discussed in the lectures [24] in 2008, the MINOS collaboration reported their first results on the search for $\nu_\mu \to \nu_e$ transitions based on an exposure of $3.14 \cdot 10^{20}$ protons-on-target in the Fermilab NuMI beam. They observed 35 events in the Far Detector with a background of $(27 \pm 5(\text{stat.}) \pm 2(\text{syst.}))$ events predicted by their measurements in the Near Detector.

The probability of appearance of ν_e in MINOS due to oscillations of ν_μ neglecting matter effects for Δm^2_{31} driven oscillations but not for Δm^2_{21} driven oscillations (for which, indeed is dominant) is

$$P_{\nu_e\nu_\mu(\bar\nu_e\bar\nu_\mu)} \simeq s^2_{23}\, \sin^2 2\theta_{13}\, \sin^2\left(\frac{\Delta m^2_{31}\, L}{4E}\right) + \\ + \tilde J\, \frac{\Delta m^2_{12}}{2EV_e}\, \sin\left(\frac{V_e L}{2}\right) \sin\left(\frac{\Delta m^2_{31} L}{4E}\right) \cos\left(\frac{\Delta m^2_{31}\, L}{4E} \pm \delta_{CP}\right), \quad (36)$$

where $\tilde J = c_{13} \sin^2 2\theta_{13} \sin^2 2\theta_{23} \sin^2 2\theta_{12}$ and the $\pm$ corresponds to neutrinos and antineutrinos, respectively.

The dominant term, the first one, is proportional to the $\sin^2(2\theta_{13})$. Thus the first MINOS results which represented a 1.5σ excess could be explained by a nonzero value of θ_{13}. There is also some mild dependence of the bound on the value of the CP phase because of the second term. Recently the analysis has been updated with double statistics (exposure of $7 \cdot 10^{20}$). They reported the observation of 54 events with an expected background of $49.1 \pm 7(\text{stat.}) \pm 2.7(\text{syst.})$. So the excess above background has reduced to 0.7σ.

4. GLOBAL 3ν ANALYSIS OF OSCILLATION DATA

The results of the global combined analysis including the SK(I+II+III) atmospheric neutrino data and all dominant and subdominant oscillation effects are summarized in Fig. 9, where we show the different projections of the allowed six-dimensional parameter space. The full regions correspond to the analysis done in the framework of the GS98 solar model and with Ga capture cross section in [35], while the void regions correspond the analysis with AGSS09 solar fluxes and the modified Ga capture cross section in [36]. The regions in each panel are obtained after marginalization of χ^2_{global} with respect to the undisplayed parameters. In the lower panel we show the allowed regions in the $(\sin^2\theta_{13},\, \delta_{CP})$ plane. As is seen in the figure, at present the sensitivity to the CP phase is marginal but we find that the bound on $\sin^2\theta_{13}$ can vary by about $\sim 30\%$ depending on the exact value of δ_{CP}. This arises mainly from the interference of θ_{13} and Δm^2_{21}

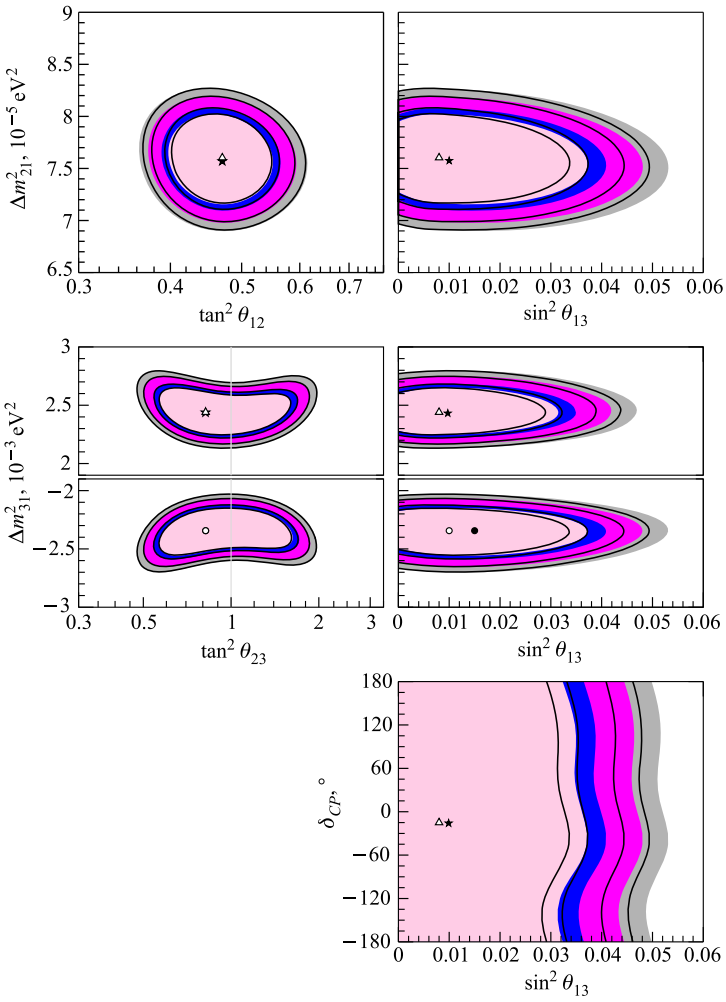

Fig. 9. Global 3ν oscillation analysis. Each panel shows two-dimensional projection of the allowed five-dimensional region after marginalization with respect to the undisplayed parameters. The different contours correspond to the two-dimensional allowed regions at 90, 95, 99 and 3σ CL. The full regions correspond to the analysis done in the framework of the GS98 solar model and with Ga capture cross section of Bahcall, while the void regions correspond to the analysis with AGSS09 solar fluxes and the modified Ga capture cross section (see [37] for details)

effects in the atmospheric neutrino observables, as well as from the new MINOS ν_e appearance data. The derived ranges for the six parameters at the 1σ (3σ) level are presented below:

GS98 with Gallium cross section from [35]	AGSS09 with modified Gallium cross section [36]
$\Delta m^2_{21} = \left(7.59 \pm 0.20 \left(^{+0.61}_{-0.69}\right)\right) \cdot 10^{-5}\ \mathrm{eV}^2$	Same
$\Delta m^2_{31} = \begin{cases} (-2.36 \pm 0.11\,(\pm 0.37)) \cdot 10^{-3}\ \mathrm{eV}^2 \\ (+2.46 \pm 0.12\,(\pm 0.37)) \cdot 10^{-3}\ \mathrm{eV}^2 \end{cases}$	Same
$\theta_{12} = \left(34.4 \pm 1.0 \left(^{+3.2}_{-2.9}\right)\right)^\circ$	$\left(34.5 \pm 1.0 \left(^{+3.2}_{-2.8}\right)\right)^\circ$
$\theta_{23} = \left(42.8^{+4.7}_{-2.9} \left(^{+10.7}_{-7.3}\right)\right)^\circ$	Same
$\theta_{13} = \left(5.6\,^{+3.0}_{-2.7}\,(\leqslant 12.5)\right)^\circ$	$\left(5.1\,^{+3.0}_{-3.3}\,(\leqslant 12.0)\right)^\circ$
$\left[\sin^2\theta_{13} = 0.0095\,^{+0.013}_{-0.007}\,(\leqslant 0.047)\right]$	$\left[0.008\,^{+0.012}_{-0.007}\ (\leqslant 0.043)\right]$
$\delta_{CP} \in [0,\, 360]$	Same

For each parameter the ranges are obtained after marginalizing with respect to the other parameters. For Δm^2_{31} the allowed ranges are formed by two disconnected intervals which correspond to the two possible mass orderings. The absolute best-fit lays in the positive $\Delta m^2_{31} = +2.46 \cdot 10^{-3}\ \mathrm{eV}^2$. The 1σ and 3σ ranges are defined with respect to this absolute minimum. In particular, the local best-fit in the inverse mass ordering, $\Delta m^2_{31} = -2.36 \cdot 10^{-3}\ \mathrm{eV}^2$, is at a $\Delta\chi^2 = 0.12$.

SUMMARY

In these lectures we have discussed the present status of the combined statistical analysis of solar, atmospheric, LBL and reactor data in the framework of neutrino oscillations. The experimental results discussed can be consistently described in the framework of oscillations between the three known neutrinos of the SM after a mass for them is included. To present date we have a good determination of the two relevant mass differences up to their relative sign, and two of the mixing angles. We have a constraint on the third mixing angle but no clear evidence on whether it is or not zero has been found. Everything else we ignore.

There are also a set of questions in the experimental results which I have not discussed but that have been addressed in other lectures. In particular, the results from MiniBooNE and MINOS $\bar{\nu}_\mu$ disappearance described in the lectures [24]. They cannot be accommodated within the 3ν oscillation picture here described. Indeed, at present there is no appealing theoretical framework to explain them.

To address these open questions a new generation of neutrino experiments are starting to take data [25] or being proposed [26]. The ultimate but immediate goal is the full determination of the low energy parametrization of the leptonic sector. The long term aim is learning more about the origin of the particle masses

and mixing, this is, about the flavour puzzle, and the underlying dynamics they originate from — as a start.

Acknowledgements. I want to thank the organizers of this school for their warm and kind hospitality during my visit to Alushta. This work is supported by Spanish MICINN grant 2007-66665-C02-01, and consolider-ingenio 2010 grant CSD-2008-0037, by CUR Generalitat de Catalunya grant 2009SGR502 and by USA-NSF grant PHY-0653342.

REFERENCES

1. *Bilenky S. M., Giunti C., Grimus W.* Phenomenology of Neutrino Oscillations // Prog. Part. Nucl. Phys. 1999. V. 43. P. 1; hep-ph/9812360.
2. *Dolgov A. D.* Neutrinos in Cosmology // Phys. Rep. 2002. V. 370. P. 333; hep-ph/0202122.
3. *Barger V., Marfatia D., Whisnant K.* Progress in the Physics of Massive Neutrinos // Intern. J. Mod. Phys. E. 2003. V. 12. P. 569; hep-ph/0308123.
4. *Pakvasa S., Valle J. W. F.* Neutrino Properties before and after KamLAND // Proc. Indian Nat. Sci. Acad. 2004. V. 70A. P. 189; hep-ph/0301061.
5. *Maltoni M. et al.* Status of Global Fits to Neutrino Oscillations // New J. Phys. 2004. V. 6. P. 122; hep-ph/0405172.
6. *Fogli G. L. et al.* Global Analysis of Three-Flavor Neutrino Masses and Mixings // Prog. Part. Nucl. Phys. 2006. V. 57. P. 742; hep-ph/0506083.
7. *Mohapatra R. N., Smirnov A. Y.* Neutrino Mass and New Physics // Ann. Rev. Nucl. Part. Sci. 2006. V. 56. P. 569; hep-ph/0603118.
8. *Lesgourgues J., Pastor S.* Massive Neutrinos and Cosmology // Phys. Rep. 2006. V. 429. P. 307; astro-ph/0603494.
9. *Strumia A., Vissani F.* Neutrino Masses and Mixings and ... hep-ph/0606054.
10. *Nunokawa H., Parke S. J., Valle J. W. F.* CP Violation and Neutrino Oscillations. hep-ph/0710.0554.
11. *Gonzalez-Garcia M. C., Nir Y.* Developments in Neutrino Physics // Rev. Mod. Phys. 2003. V. 75. P. 345; hep-ph/0202058.
12. *Gonzalez-Garcia M. C., Maltoni M.,* Phenomenology with Massive Neutrinos // Phys. Rep. 2008. V. 460. P. 1; hep-ph/0704.1800.
13. *Bahcall J. N.* Neutrino Astrophysics. Cambridge Univ. Press, 1989.
14. *Boehm F., Vogel P.* Physics of Massive Neutrinos. Cambridge Univ. Press, 1987.
15. *Kayser B., Gibrat-Debu F., Perrier F.* The Physics of Massive Neutrinos // World Sci. Lect. Notes Phys. 1989. V. 25. P. 1.
16. *Gaisser T. K.* Cosmic Rays and Particle Physics. Cambridge Univ. Press, 1990.
17. *Kim C.W., Pevsner A.* Neutrinos in Physics and Astrophysics // Contemp. Concepts Phys. 1993. V. 8. P. 1.
18. *Mohapatra R. N., Pal P. B.* Massive Neutrinos in Physics and Astrophysics. 2nd ed. // World Sci. Lect. Notes Phys. 1998. V. 60. P. 1; 2004. V. 72. P. 1.

19. *Fukugita M., Yanagida T.* Physics of Neutrinos and Applications to Astrophysics. Berlin: Springer, 2003.
20. See lectures by *Grimus W.* // Part. Nucl., Lett. 2011. V. 8, No. 7(170).
21. See lectures by *Bilenky S.* // Ibid.
22. See lectures by *Chen M.* // Ibid.
23. See lectures by *Suzuki Y.* // Ibid.
24. See lectures by *Wojcicki S.* // Ibid.
25. See lectures by *Pouttisou J. M.* // Ibid.
26. See lectures by *Mezzetto M.* // Ibid.
27. *Maki Z., Nakagawa M., Sakata S.* Remarks on the Unified Model of Elementary Particles // Prog. Theor. Phys. 1962. V. 28. P. 870.
28. *Schechter J., Valle J. W. F.* Neutrino Masses in $SU(2)\times U(1)$ Theories // Phys. Rev. D. 1980. V. 22. P. 2227.
29. *Schechter J., Valle J. W. F.* Comment on the Lepton Mixing Matrix // Ibid. V. 21. P. 309.
30. *Schechter J., Valle J. W. F.* Majorana Neutrinos and Magnetic Fields // Phys. Rev. D. 1981. V. 24. P. 1883; Erratum // Phys. Rev. D. 1982. V. 25. P. 283.
31. *Kobayashi M., Maskawa T.* CP Violation in the Renormalizable Theory of Weak Interaction // Prog. Theor. Phys. 1973. V. 49. P. 652.
32. *Bahcall J. N. et al.* Helioseismological Implications of Recent Solar Abundance Determinations // Astrophys. J. 2005. V. 618. P. 1049; astro-ph/0407060.
33. *Serenelli A. et al.* New Solar Composition: The Problem with Solar Models Revisited. astro-ph.SR/0909.2668.
34. *Gonzalez-Garcia M. C., Maltoni M., Salvado J.* Direct Determination of the Solar Neutrino Fluxes from Solar Neutrino Data // JHEP. 2010. V. 1005. P. 072.
35. *Bahcall J. N.* Gallium Solar Neutrino Experiments: Absorption Cross Sections, Neutrino Spectra, and Predicted Event Rates // Phys. Rev. C. 1997. V. 56. P. 3391–3409.
36. *Abdurashitov J. N. et al. (SAGE Collab.).* Measurement of the Solar Neutrino Capture Rate with Gallium Metal. III: Results for the 2002–2007 Data-Taking Period // Phys. Rev. C. 2009. V. 80. P. 015807.
37. *Gonzalez-Garcia M. C., Maltoni M., Salvado J.* Updated Global Fit to Three Neutrino Mixing: Status of the Hints of $\theta_{13} > 0$ // JHEP. 2010. V. 1004. P. 056; hep-ph/1001.4524.
38. *Apollonio M. et al. (CHOOZ Collab.).* Limits on Neutrino Oscillations from the CHOOZ Experiment // Phys. Lett. B. 1999. V. 466. P. 415–430.
39. *Fogli G. L. et al.* Hints of $\theta_{13} > 0$ from Global Neutrino Data Analysis // Phys. Rev. Lett. 2008. V. 101. P. 141801.